SNPP ATMS On-Orbit Geolocation Error Evaluation and Correction Algorithm

Jun Zhou, *Member, IEEE,* Hu Yang, *Member, IEEE*, and Kent Anderson

***Abstract*— For the quantitative applications of the Suomi National Polar-orbiting Partnership (SNPP) Advanced Technology Microwave Sounder (ATMS), the geolocation accuracy of its sensor data records must be quantified during its on-orbit operation. In this paper, a refined coastline inflection point method is used to evaluate the on-orbit geolocation accuracy of SNPP ATMS. It is disclosed that for SNPP ATMS, the static error term with scan-angle-dependent feature is a dominant part among all the geolocation error sources. A mathematical model is then developed to convert the in-track and cross-track geolocation errors to the beam pointing Euler angles defined in the spacecraft coordinate system, which can be further used to construct the correction matrix for on-orbit geolocation process. By using the correction matrix built in this paper, the geolocation error is obviously reduced both at nadir and at the edge of the scan. The total geolocation error at nadir before/after correction is 3.8/0.8 km at K-band, 5.6/0.8 km at Ka-band, 3.3/0.4 km at V-band, and 1.5/0.1 km at W-band. The geolocation bias at the edge of the scan line before/after correction is 4.6/1.3 km at K-band, 9.4/1.8 km at Ka-band, 4.4/2.4 km at V-band, and 3.2/0.8 km at W-band. After correction, the scan-angle-dependent feature in geolocation error is also largely reduced.**

***Index Terms*— Advanced Technology Microwave Sounder (ATMS), coastline inflection point(CIP), Euler angles, geolocation error, microwave radiometer, Suomi National Polar-orbiting Partnership (SNPP).**

I. Introduction

THE Suomi National Polar-orbiting Partnership (SNPP) satellite carried the Advanced Technology Microwave Sounder (ATMS) on board, and it was successfully launched into orbit at about 839 km above the earth with an inclination angle of 98.7°. The ATMS is a cross-track scanning microwave radiometer. It scans ±52.725° from nadir to complete a total of 96 fields of view (FOVs) along scan lines. ATMS has a swath width of 2700 km, which leaves almost no data gap even near the Equator. A total of 22 channels at microwave frequency ranging from 23 to 183 GHz are configured at ATMS. The beam widths of channels 1–2, 3–16, and 17–22 are 5.2°, 2.2°, and 1.1°, respectively, which correspond to the FOV sizes about 75, 32, and 16 km at nadir. More details about ATMS instrument can be obtained from [1] and [2]. For an optimal use of ATMS observations in weather and climate research and applications, high geolocation accuracy is required.

In operational geolocation process, ATMS geolocation is calculated from an instrument geolocation module and a common geolocation module. In the instrument geolocation module, the sensor exit vector in the antenna coordinate system is built from scan angle and then transformed to the spacecraft coordinate (SC) system by applying the beam misalignment correction matrix and the instrument mounting matrix. In the common geolocation module, the corrected vector goes through further corrections for satellite attitude perturbation and the earth orientation such as polar wander, procession, and nutation. The geodetic latitude and longitude for each FOV can then be derived from the intersection of the corrected sensor exit vector with earth surface in the Earth Centered and Earth Fixed coordinate system (ECEF). Note that, ATMS has two receiving antennas: one receiving antenna serving for channels 1–15 with frequencies below 60 GHz and the other for channels 16–22 with frequencies above 60 GHz. The antenna beam pointing direction is differentiated into five bands: K- (channel 1), Ka- (channel 2), V- (channels 3–15), W- (channel 16), and G- (channels 17–22) bands. Each band has its own set of latitude and longitude at each beam position. For the detailed relationship between all the frames in geolocation process, please refer to [3, Table I]. The designed boresight pointing accuracy of SNPP ATMS is about 0.3°, 0.2°, and 0.1° for K-/Ka-band (channels 1–2), V-/W-band (channels 3–16), and G-band (channels 17–22), respectively [2]. They can be translated to ground geolocation error of 4.3, 2.9, and 1.4 km at nadir.

For SNPP ATMS, the static error originates from the antenna beam misalignment and the instrument mounting error is the dominant part in the total geolocation error. During the antenna subsystem verification test, the antenna beam alignment with respect to the instrument cube was measured as Euler angle roll and pitch for each channel at three different scan positions (FOV-1, 48, and 96) and they are further interpolated to the other FOV positions. Instrument mounting error is defined as the misalignment between the instrument and the SC systems. It is measured in terms of Euler angle roll, pitch, and yaw during prelaunch ground test, from which the mounting matrix can be constructed and provided to rotate the instrument view vector from the instrument frame to the

Manuscript received July 18, 2017; revised November 12, 2017, May 23, 2018, August 20, 2018, November 21, 2018, and December 8, 2018; accepted December 13, 2018. Date of publication January 24, 2019; date of current version May 28, 2019. *(Corresponding author: Hu Yang.)*

J. Zhou and H. Yang are with the Earth System Science Interdisciplinary Center, University of Maryland, College Park, MD 20740 USA (e-mail: jzhou128@umd.edu; huyang@umd.edu).

K. Anderson is with Northrop Grumman Electronic Systems, Azusa, CA 91702 USA.

Color versions of one or more of the figures in this paper are available online at http://ieeexplore.ieee.org.

Digital Object Identifier 10.1109/TGRS.2018.2887407

control frame of the spacecraft [4]. Even though these static error terms have been measured in the prelaunch ground test and the corrections have been included in geolocation process, residual errors may still exist due to the on-orbit thermal dynamic change and shift during the launch. Therefore, post-launch assessment and correction for static errors are necessary for improving the on-orbit geolocation accuracy.

Several methods were developed to assess the on-orbit geolocation error, such as coastline inflection point (CIP) method [5]–[8], image co-registration method [9]–[13], land–sea fraction method [14], and ascending and descending observation comparison [15]. While most of the above-mentioned research is focused on assessing the on-orbit geolocation errors, some studies also attempted to retrieve the boresight pointing Euler angles defined in certain frames from the estimated geolocation error [15]–[17]. Most of the approaches are based on empirical method, in which the Euler angles are obtained through tuning the pitch, roll, and yaw angle iteratively until the geolocation error is minimized. Moradi *et al.* [15] found that the tuning order of the three angles had some impact on the retrieval result. This may lead to nonunique solutions and results in the nonconvergence problem. Besides, the empirical method is time-consuming; it is a trial-and-error process that does not use the derivative of the objective function.

In our previous study, a geolocation mathematical model along with CIP method was developed and applied to retrieve the boresight pointing Euler angles in a specifically defined spacecraft body frame for FengYun-3C microwave radiation imager [3] and SNPP ATMS [2]. It is found that several factors such as small islands and cloud contamination can affect the accuracy of CIP method [6], [17]. Such bias in the data and its effect to the retrieval result has never been investigated before. In addition, the scan-angle-dependent antenna beam misalignment may not be completely removed in geolocation process by using the beam offset angles measured in the prelaunch ground test. This can lead to scan-angle-dependent error in geolocation results which cannot be corrected by a single set of Euler angles.

In this paper, to address the problems mentioned above, the retrieval algorithm for correcting the static geolocation error of SNPP ATMS is improved. A modified mathematical model for connecting the ground geolocation error to the boresight pointing Euler angles in SC system is introduced in Section II. The on-orbit geolocation error of SNPP ATMS is evaluated through a refined CIP method in Section III. A retrieval algorithm based on the mathematical model and the refined CIP method is developed in Section IV, followed by its application on SNPP ATMS. In Section V, the retrieved Euler angles in spacecraft frame are used to construct the on-orbit correction matrices, and their application results are validated. Conclusion and discussion are presented in Section VI.

II. Refined Geolocation Error Mathematical Model

In this section, a mathematical model for correcting boresight pointing error is introduced. This model is built in SC system defined in the operational geolocation process, which makes it convenient to be implemented into the on-orbit geolocation program. This mathematical model builds the foundation for the development of the retrieval algorithm in Sections II-A and II-B.

A. Boresight Pointing Error Correction Model

For ATMS, the scan is performed in yz plane of the antenna coordinate system. The beam vector is initially generated as a function of scan angle ϑ

$$\vec{b}_{\mathrm{Ant}} = \begin{bmatrix} 0 \\ \sin\vartheta \\ \cos\vartheta \end{bmatrix}. \tag{1}$$

In geolocation process, $\vec{b}_{\mathrm{Ant}}$ is transformed all the way to the beam vector in ECEF by multiplying a series of rotation matrices

$$\vec{b}_{\mathrm{ECEF}} = \mathrm{ROT}_{\mathrm{ECEF/ECI}}\mathrm{ROT}_{\mathrm{ECI/SC}}\mathrm{ROT}_{\mathrm{SC/Inst}}\mathrm{ROT}_{\mathrm{Inst/Ant}}\vec{b}_{\mathrm{Ant}} \tag{2}$$

where $\mathrm{ROT}_{B/A}$ is the rotation matrix transforming beam vector from the coordinate system A to B. The ground location of FOV is obtained from the intersection of $\vec{b}_{\mathrm{ECEF}}$ and WGS84 reference frame [18]. As mentioned in Section I, the Euler angle roll and pitch that create $\mathrm{ROT}_{\mathrm{Inst/Ant}}$ are scan-angle-dependent. Thus, the matrix $\mathrm{ROT}_{\mathrm{Inst/Ant}}$ also has scan-angle-dependent feature.

In our previous study, the geolocation error mathematical model was developed for the conversion between the ground geolocation error and the boresight pointing error in a specifically defined spacecraft body frame [3]. This frame is similar to SC system in the operational geolocation process, except that its y-axis is normal to the satellite velocity vector in ECEF rather than Earth-centered Inertial coordinate system (ECI). Further study shows that the beam vector in this frame is slightly affected by the time-varying earth movement and this could result in some retrieval uncertainty. Besides, the retrieved boresight pointing Euler angles defined in this frame cannot be directly applied into the operational geolocation process. In this paper, the geolocation error mathematical model is improved. This mathematical model is now established in SC system defined in the operational geolocation procedure, and therefore, the correction matrix constructed by the retrieved Euler angles can be directly applied to the operational geolocation process.

Fig. 1 shows the geolocation error caused by the misalignment between SC and the instrument coordinate system (INST). This misalignment is measured in three Euler angles of roll, pitch, and yaw, which are defined as the rotation around x-, y-, and z-axes of SC, respectively. In Fig. 1, for brevity, only the rotation of INST about x-axis of the SC by roll is presented. Given $\vec{b'}_{\mathrm{SC}}$ and $\vec{b}_{\mathrm{SC}}$ are the true and the observed unit beam vectors in SC, A and B are intersection points of these two unit vectors with the earth ellipsoid. Since the antenna beam misalignment in terms of Euler angle roll and pitch is scan-angle-dependent and the prelaunched determined $\mathrm{ROT}_{\mathrm{Inst/Ant}}$ may not be able to correct it completely, the remaining of such error will make the

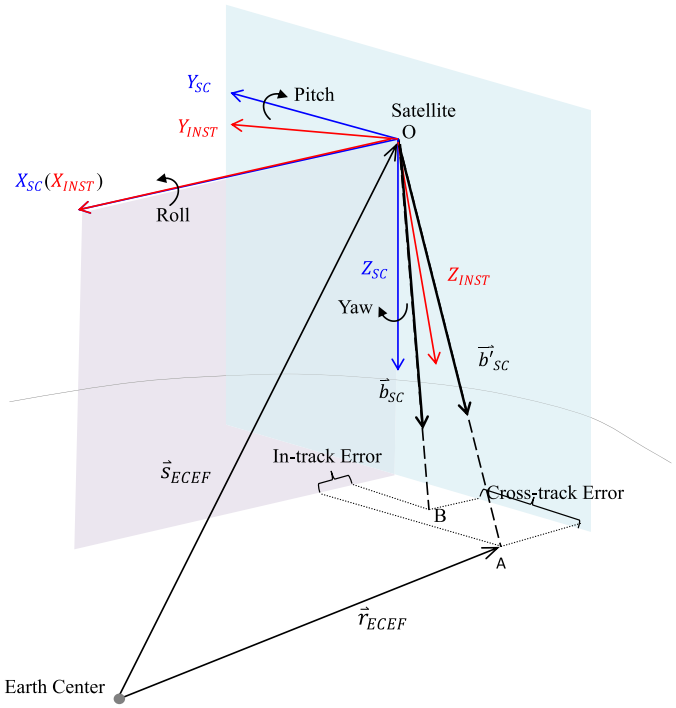

Fig. 1. Schematic illustration of the mathematical model. x_{SC}, y_{SC}, and z_{SC} are the axes of SC. x_{INST}, y_{INST}, and z_{INST} are the axes of INST. $\vec{b}_{\mathrm{SC}}$ and $\vec{b}'_{\mathrm{SC}}$ are the true and the observed unit beam vectors, and A and B are their corresponding FOVs. In-track and cross-track errors are the projection of the total geolocation error between A and B onto the along-track and cross-track directions.

total static boresight pointing error has a scan-angle-dependent feature that cannot be accurately corrected by a single set of Euler angle roll, pitch, and yaw. Therefore, the correction of such boresight pointing error should be made at each FOV position by Euler angle roll and pitch defined in SC at that specific scan angle

$$\vec{b}'_{\mathrm{SC}} = \mathrm{ROT}_{\mathrm{corr}} \cdot \vec{b}_{\mathrm{SC}} \tag{3}$$

where $\mathrm{ROT}_{\mathrm{corr}}$ is the correction matrix and its elements are defined by Euler angles ξ_{r} and ξ_{p}

$$\mathrm{ROT}_{\mathrm{corr}} = \mathrm{ROT}_{\mathrm{r}}(\xi_{\mathrm{r}}) \cdot ROT_{\mathrm{p}}(\xi_{\mathrm{p}}) \tag{4a}$$

$$\mathrm{ROT}_{\mathrm{r}}(\xi_{\mathrm{r}}) = \begin{bmatrix} 1 & 0 & 0 \\ 0 & \cos\xi_{\mathrm{r}} & -\sin\xi_{\mathrm{r}} \\ 0 & \sin\xi_{\mathrm{r}} & \cos\xi_{\mathrm{r}} \end{bmatrix} \tag{4b}$$

$$\mathrm{ROT}_{\mathrm{p}}(\xi_{\mathrm{p}}) = \begin{bmatrix} \cos\xi_{\mathrm{p}} & 0 & \sin\xi_{\mathrm{p}} \\ 0 & 1 & 0 \\ -\sin\xi_{\mathrm{p}} & 0 & \cos\xi_{\mathrm{p}} \end{bmatrix}. \tag{4c}$$

The Euler angle yaw is not included in the correction model, since the cross-track and in-track errors caused by yaw at a certain FOV can be mitigated by roll and pitch at that position. This paper aims to measure and correct the boresight pointing error in terms of Euler angles defined in SC system. The Euler angles appear in the remainder of this paper are all defined in that frame unless mentioned otherwise.

B. Conversion From ECEF to Spacecraft Coordinate System

Since the geolocation error can only be derived from the geodetic latitude/longitude of ground targets, in order to apply (3), the ground point location needs to be transferred to the beam vector in SC. The transformation is an inverse process of the operational geolocation procedure following (2). The detailed procedure is described in the following.

As shown in Fig. 1, given $(\lambda_{\mathrm{c}}, \varphi_{\mathrm{c}})$ is the geocentric longitude and latitude for ground point A, its corresponding ground location vector $\vec{r}_{\mathrm{ECEF}}$ in ECEF can be expressed as

$$\vec{r}_{\mathrm{ECEF}} = |\vec{r}_{\mathrm{ECEF}}| \begin{bmatrix} \cos\varphi_{\mathrm{c}}\cos\lambda_{\mathrm{c}} \\ \cos\varphi_{\mathrm{c}}\sin\lambda_{\mathrm{c}} \\ \sin\varphi_{\mathrm{c}} \end{bmatrix} \tag{5}$$

where $|\vec{r}_{\mathrm{ECEF}}|$ can be obtained through the ellipsoid parameter equation

$$|\vec{r}_{\mathrm{ECEF}}| = \sqrt{\frac{(a \cdot b)^2}{(a \cdot \sin\varphi_{\mathrm{c}})^2 + (b \cdot \cos\varphi_{\mathrm{c}})^2}} \tag{6}$$

where a and b are the equatorial radius and polar radius of earth. Given $\vec{s}_{\mathrm{ECEF}}$ is the satellite position vector in ECEF, which is defined as a vector pointing from the center of earth to the mass center of satellite, the beam vector $\vec{b}_{\mathrm{ECEF}}$ can be determined from trigonometry of the view vector $\vec{s}_{\mathrm{ECEF}}$ and $\vec{r}_{\mathrm{ECEF}}$ as

$$\vec{b}_{\mathrm{ECEF}} = \vec{r}_{\mathrm{ECEF}} - \vec{s}_{\mathrm{ECEF}}. \tag{7}$$

To accomplish the transformation from ECEF to ECI, it is necessary to form four matrices. These are the precession matrix, the astronomic nutation matrix, the sidereal time matrix, and the polar motion matrix [19]. The earth orientation parameters are provided by IERS (https://www.iers.org/IERS/EN/DataProducts/EarthOrientationData/eop.html). The product of these matrices forms the rotation matrix $R_{\mathrm{ECI/ECEF}}$ which transforms $\vec{b}_{\mathrm{ECEF}}$ to $\vec{b}_{\mathrm{ECI}}$

$$\vec{b}_{\mathrm{ECI}} = R_{\mathrm{ECI/ECEF}} \cdot \vec{b}_{\mathrm{ECEF}}. \tag{8}$$

The transformation is accomplished by using the Naval Observatory Vector Astrometry Software Package version F3.1, which is an open source library for computing various commonly used quantities in positional astronomy [20]. $\vec{s}_{\mathrm{ECEF}}$ and the satellite velocity $\vec{v}_{\mathrm{ECEF}}$ can be transformed to $\vec{s}_{\mathrm{ECI}}$ and $\vec{v}_{\mathrm{ECI}}$ in the same way, except that the earth's rotation should be taken into account when converting the velocity vector. $\vec{s}_{\mathrm{ECI}}$ and $\vec{v}_{\mathrm{ECI}}$ are then used to build the rotation matrix from ECI to the orbital (Orb) coordinate system. The origin of Orb system is the spacecraft center of mass with the z-axis pointing to nadir. The y-axis is the normalized cross product of the z-axis and $\vec{v}_{\mathrm{ECI}}$. The x-axis is the cross product of the y- and z-axes [18]. By defining the axes of Orb in ECI, the transformation matrix from ECI to Orb can be built

as follows:

$$\vec{z} = \begin{bmatrix} -\cos\varphi_{SC}\cos\lambda_{SC} \\ -\cos\varphi_{SC}\sin\lambda_{SC} \\ -\sin\varphi_{SC} \end{bmatrix} \tag{9a}$$

$$\vec{y} = \frac{\vec{z} \times \vec{v}_{ECI}}{|\vec{z} \times \vec{v}_{ECI}|} \tag{9b}$$

$$\vec{x} = \vec{y} \times \vec{z} \tag{9c}$$

$$\mathrm{ROT}_{Orb/ECI} = \left[\vec{x}\ \vec{y}\ \vec{z}\right]^{T} \tag{9d}$$

where $(\lambda_{SC}, \varphi_{SC})$ is the satellite geodetic location which can be obtained from $\vec{s}_{ECEF}$ in an iterative way [19]. To further transform the beam vector from Orb to SC, the satellite attitude needs to be taken into account. These attitude data are provided in terms of Euler angles in ATMS SDR geolocation product at the middle time of each scan line. The Euler angles need to be transformed to quaternions and interpolated to the observation time of each FOV. The beam vector in Orb can be transformed to SC through the transformation matrix built by the interpolated quaternions

$$\vec{b}_{SC} = \mathrm{ROT}_{SC/Orb} \cdot \vec{b}_{Orb}. \tag{10}$$

The above process is the method used in this paper to transform the ground point to the beam vector in SC. The required variables, such as $\vec{s}_{ECEF}$, $\vec{v}_{ECEF}$, satellite attitude, and observation time, can be obtained from ATMS SDR geolocation product and temperature data record (TDR) product. Through this transformation process, the time-varying dynamic error arising from the earth orientation and satellite attitude is corrected.

The mathematical model in (3) and the conversion from the ground geolocation point to the beam vector in SC are the foundation of the subsequent geolocation error evaluation and retrieval algorithm for the boresight pointing Euler angles of SNPP ATMS.

III. On-Orbit Geolocation Error Evaluation

In this paper, CIP method is adopted to evaluate the on-orbit geolocation error. In CIP method, any four consecutive observations are fit employing a cubic polynomial function. The inflection point of the fit line is considered as an observed coastline point only when it falls between the second and third measurements and when the difference between the second and third measurements exceeds 10 K. The 10-K threshold is determined through sensitivity studies. The corresponding ground "truth" is defined as the point at the true coastline that nearest to it. The locations of the true coastlines are provided by Global Self-consistent, Hierarchical, High-resolution Geography Database (GSHHG) version 2.3.6 released on August 19, 2016 [21].

Using the basic CIP method to evaluate the on-orbit geolocation error will cause large uncertainties as mentioned in Section I. In order to reduce the bias in the samples, some improvements have been made to the traditional CIP method. The improved method is applied to SNPP ATMS observations to assess the on-orbit geolocation error. The root cause of the scan-angle-dependent feature observed in geolocation error is then studied based on the estimated in-track and cross-track errors.

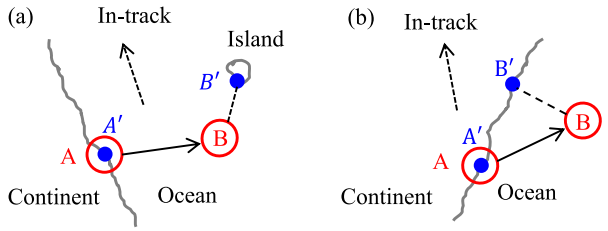

Fig. 2. Schematic illustration of the mismatch of ground truth and observed ground location caused by the (a) contamination of islands and the (b) orientation of a coastline. The red circle represents the observed ground point A and it moves to B along the solid line with arrow due to boresight pointing error. The blue points A′ and B′ represent the "true" coastline points identified by CIP method before and after the movement of the observed point.

A. Improvement of Coastline Inflection Point Method

As discussed in Section I, when the CIP method is applied to determine the "true" ground geolocation point, the presentation of clouds and islands as well as the coastline orientation will lead to uncertainties in the "true" coastline points. As shown in Fig. 2, the coastline point is observed at point A provided that the instrument beam vector is accurate. But if the boresight pointing error presents, the observed coastline point will move from point A to point B along the solid line with arrow. In CIP method, the ground "truth" is determined as the coastline point that closest to the measured one. This will lead to the identification of an incorrect "true" coastline point under the following situations. As shown in Fig. 2(a), if there is a small island that closer to B than A, the "true" point will be located at B′ instead of the true position A′. This issue consequently makes the magnitude of estimated geolocation error smaller than the truth, or even lead to a totally opposite sign. As shown in Fig. 2(b), if the coastline is not perpendicular to the moving direction represented by the solid line with arrow, the "true" point will be wrongly located at B′, since B′ B is shorter than A′ B. This will lead to the underestimation of geolocation error. Besides, the existence of clouds will either obscure coastline detections or introduce false detections, which leads to uncertainty in the retrieval samples.

In this paper, two strategies are adopted to address the issues mentioned above. First, only the coastline regions without small islands are selected, and VIIRS cloud mask product (terrain corrected) is utilized to screen out the cloud contaminated ATMS observations over the selected regions. Second, the coastlines along in-track or cross-track directions are selected to avoid the uncertainty in samples. As shown in Fig. 3, red circles B and A are the observed coastline point with and without beam pointing error. C is the "true" coastline point determined by CIP method on GSHHG. From the samples B and C identified around the coastline along in-track/cross-track directions, the cross-track/in-track error at this FOV can be estimated. This strategy is called separate-domain technique hereafter.

B. Evaluation of On-Orbit Geolocation Error

SNPP ATMS TDR in June, July, and August of 2016 (data set 2016) are used to estimate the on-orbit geolocation error

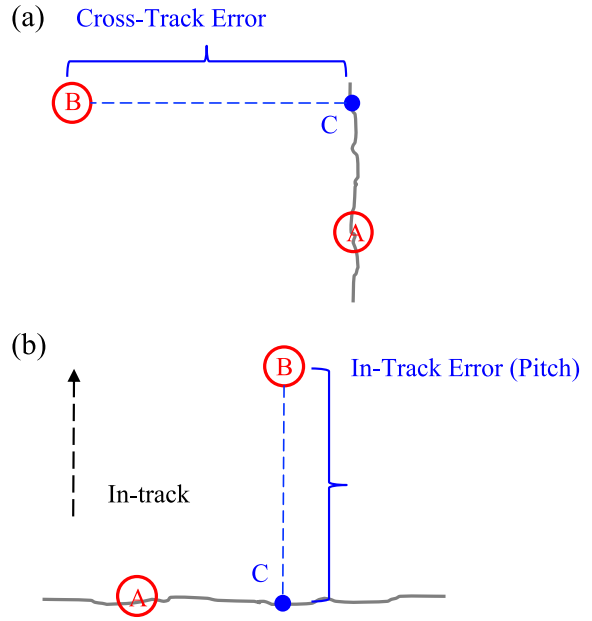

Fig. 3. Schematic illustration of the method to derive the (a) cross-track and (b) in-track geolocation errors at a certain FOV. Red circles B and A are the observed coastline point with and without beam pointing error, and blue point C is the "true" coastline point identified by CIP method on GSHHS. The other symbols have the same meaning as those in Fig. 2.

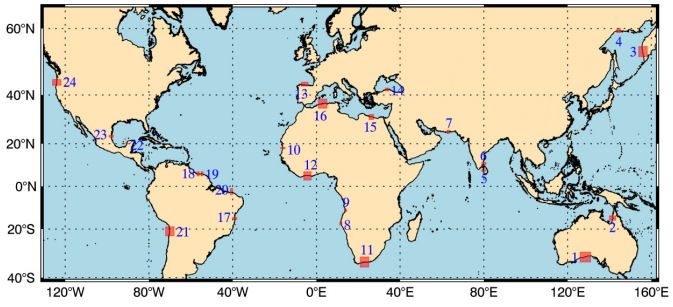

Fig. 4. Distribution of the selected 24 regions on the map.

through the refined CIP method. The collocated VIIRS cloud mask products are used to find the clear-sky observations, and GSHHG data set is taken as the true coastlines. Total of 24 regions with smooth coastline are selected, including 12 coastlines aligned with in-track direction and 12 coastlines aligned with cross-track direction. These regions are marked on map in Fig. 4. For the coastline along in-track direction, the search of inflection points is carried out along cross-track direction and vice versa. Currently, terrain correction is not included in the operational SNPP ATMS geolocation algorithm. To reduce the geolocation error caused by terrain variation, the correction process is applied to the TDR data before they are used in this paper. The surface height above the WGS84 ellipsoid is calculated by adding the mean sea level surface height data (SRTM 30 version 2) and the Ellipsoid-Geoid Separation data (EGM96). The detailed terrain correction process can be referred to [22].

ATMS antenna beam pointing direction is divided into five groups: channels 1, 2, 3–15, 16, and 17–22. Since channels 17–22 are atmosphere opaque channels, where CIP is

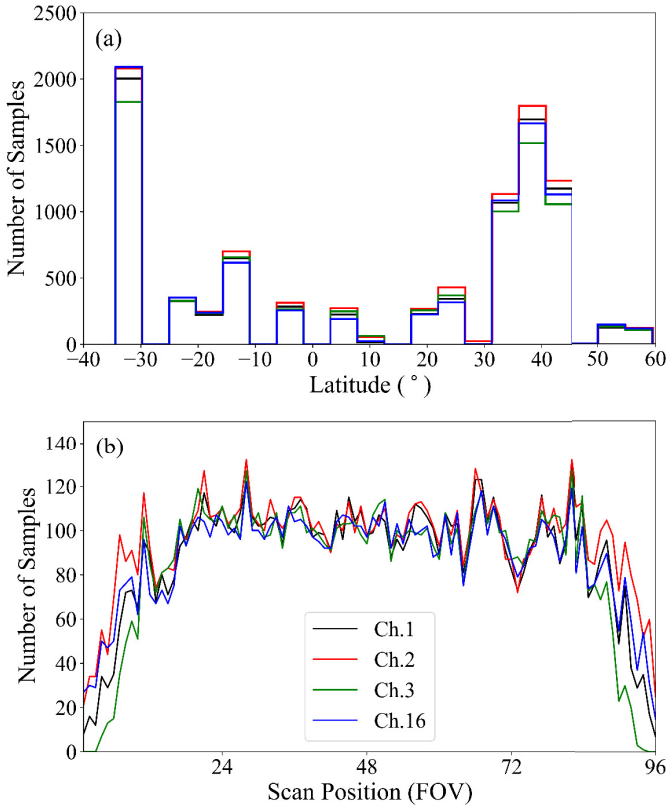

Fig. 5. Number distribution of the qualified retrieval samples of data set 2016 on (a) latitude and (b) scan positions.

not applicable, the CIP method is only applied to the observations of channels 1, 2, 3, and 16. The number distributions of the samples qualified for retrieval on regions, latitude, and scan positions are presented in Table I and Fig. 5. Table I and Fig. 5(a) show that most of the measured points concentrate around middle latitude. Fig. 5(b) shows that the number of qualified samples declines sharply toward the ends of a scan line. This is due to the overlap issue of the large FOVs at high scan angles. Two cases of the observed coastline points identified by the separate-domain technique are shown in Fig. 6. The on-orbit in-track and cross-track errors estimated by the refined CIP method are presented in Fig. 7. It can be seen that the in-track error and cross-track error show obvious scan-angle-dependent feature, especially at channels 2 and 3. The total geolocation error at nadir is estimated to be 3.6 km at K-band, 5.5 km at Ka-band, 3.4 km at V-band, and 1.6 km at W-band, which is close to the prelaunch established specification for ATMS.

C. Root Cause of Scan-Angle-Dependent Feature in Geolocation Error

Theoretically, the scan-angle-dependent feature observed in geolocation error could be caused either by the instrument mounting error expressed as a single set of Euler angle roll, pitch, and yaw or the antenna beam misalignment expressed as scan-angle-dependent roll and pitch or both. To find out the root cause, the sensitivity of in-track and cross-track geolocation errors to Euler angle roll, pitch, and yaw is studied through the following experiment. An arbitrary scan line from ATMS

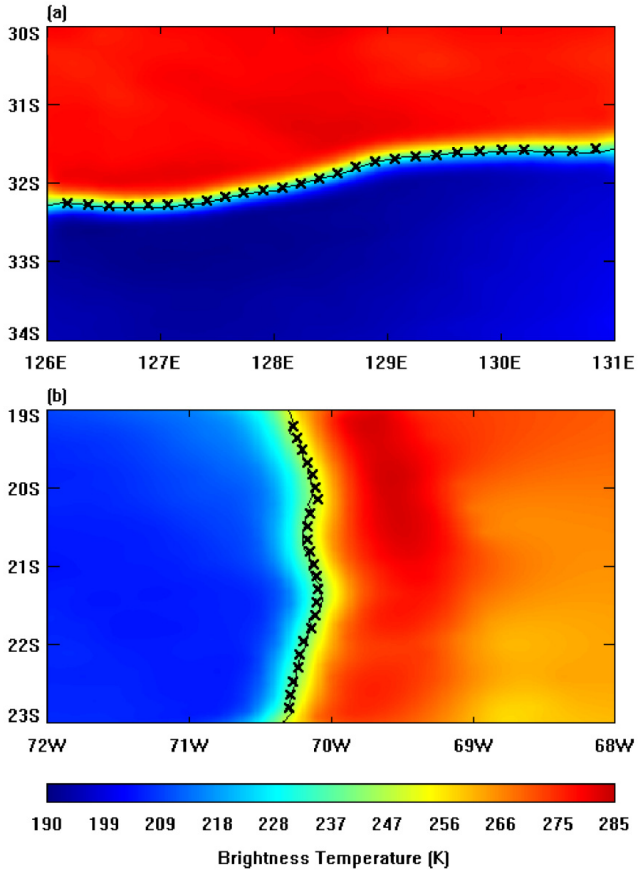

Fig. 6. Observed coastline points identified by CIP method from ATMS channel 16 TDR of July 2016 in (a) region 1 and (b) region 21. Black cross symbol represents the observed point and black solid curve is the real coastline.

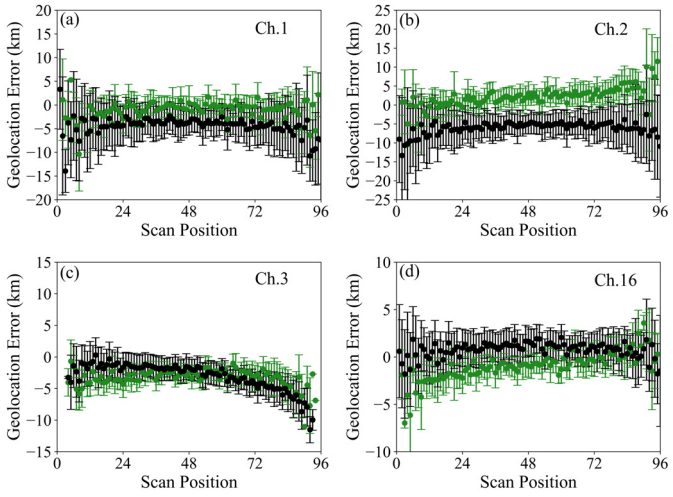

Fig. 7. FOV-dependent in-track (black points with error bar) and cross-track (green points with error bar) geolocation errors of SNPP ATMS channel 1(a), 2(b), 3(c), and 16(d) estimated from data set 2016 through the refined CIP method.

SDR geolocation file is adopted and taken as the true geolocation position. Geodetic latitude and longitude of each FOV at the scan line is used to determine the view vector in SC system following (5)–(10). Then, the vector is perturbed by adding the boresight pointing error in terms of roll/pitch/yaw angles through (3) and (4). The perturbed view vector is transformed back to the observed FOV following the operational geolocation process shown in (2). The geolocation errors along east and north directions can be calculated from the ground locations of the FOVs before and after the perturbation. These errors are further projected to the in-track and cross-track directions following the method in [2]. The perturbation of the three Euler angles is set from $-1°$ to $1°$ at an interval of $0.2°$. When one of them is tested, the other two are set to be 0. The result is presented in Fig. 8. It is noticed that in Fig. 8(a), roll alone produces small in-track geolocation error. This is because of the fact that after the application of beam alignment matrix $R_{\text{Inst/Ant}}$ and instrument mounting matrix $R_{\text{SC/Inst}}$, the beam vector is no longer in the yz plane of spacecraft frame. Therefore, a roll error will introduce the geolocation error in both in-track and cross-track directions.

The comparison among Fig. 8(b), (d), and (e) shows that the cross-track error is mainly caused by roll. If produced by a single roll angle, the geolocation error along cross-track direction should be evenly symmetric about nadir, as shown in Fig. 8(b). But, the cross-track error estimated from the raw geolocation data of SNPP ATMS in Fig. 7 exhibits more complex pattern. The cross-track error of channel 1 appears symmetry pattern, which indicates that the instrument mounting error is the main error source. As for the other three channels, the asymmetry pattern of cross-track error is quite obvious, which indicates that the antenna beam misalignment plays a major role in producing the geolocation error. This experimental result discloses that the root cause of the scan-angle-dependent geolocation error is the combination effects of both antenna beam misalignment and instrument mounting error. To correct such geolocation error, the Euler angle roll and pitch need to be determined at each FOV.

IV. Retrieval Algorithm for Boresight Pointing Euler Angles

A retrieval algorithm for the boresight pointing error in terms of Euler angles is developed based on the mathematical model along with the refined CIP method. This new retrieval algorithm is capable of reducing the bias in the samples caused by small islands, cloud, and the coastline direction. It also takes into account the scan-angle dependent feature in the boresight pointing error.

A. Retrieval Algorithm Development

Based on the analysis in Section III, the on-orbit geolocation error of SNPP ATMS has obvious scan-angle-dependent feature which cannot be corrected by a single set of Euler angles. Therefore, the retrieval algorithm developed in this section will derive the Euler angle roll and pitch at each FOV. The Euler angle yaw is not included in the retrieval, since the in-track and cross-track errors caused by yaw can be mitigated by roll and pitch at each FOV.

Provided that enough samples of observed points and their corresponding ground truth can be found, the boresight pointing error in Euler angles can be retrieved through minimizing the objective function built from (3). To reduce the bias in samples caused by small islands, cloud, and coastline direction, the refined CIP method with separate-domain technique used in geolocation error assessment in Section III is

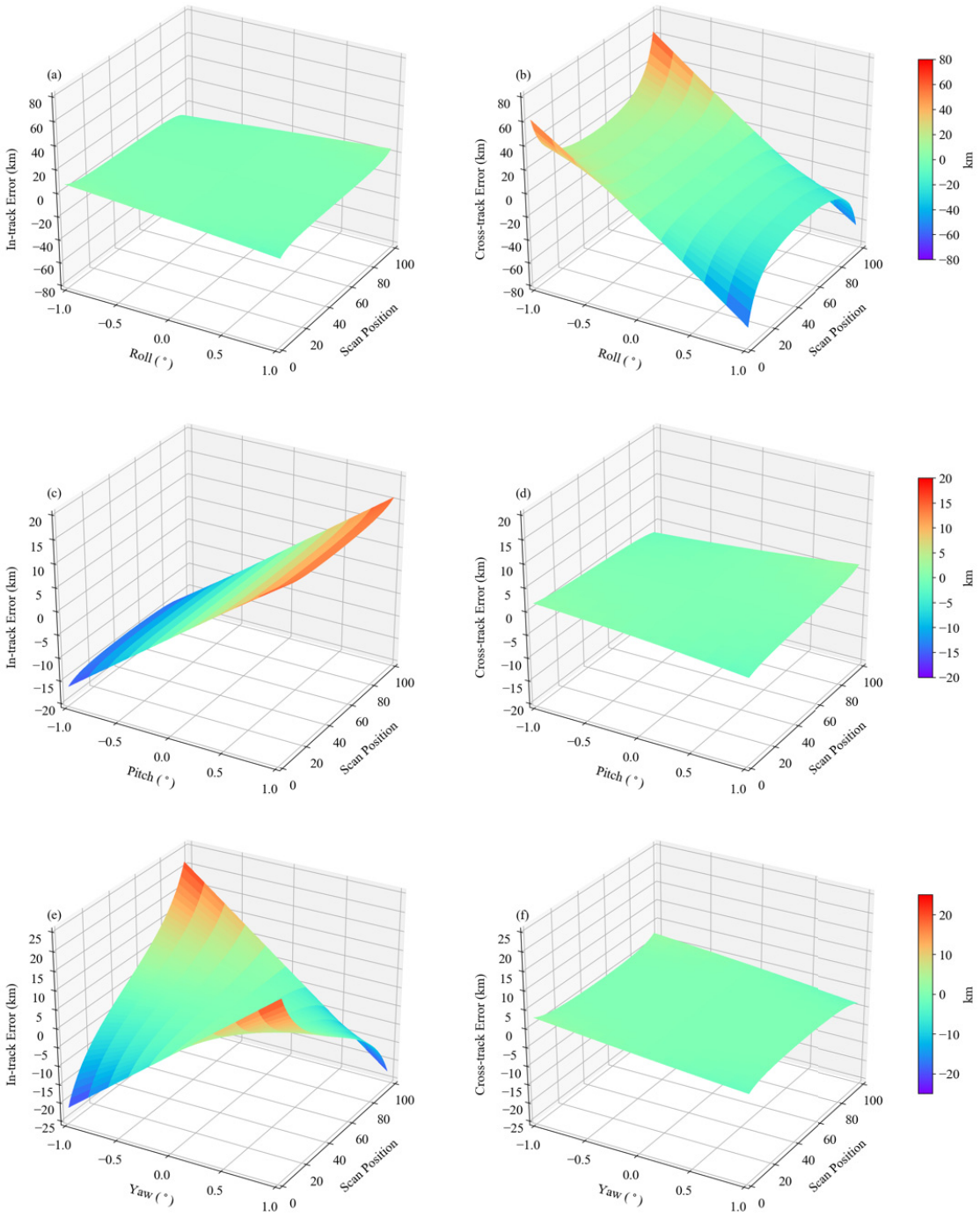

Fig. 8. Sensitivity of in-track and cross-track geolocation errors to the boresight pointing (a) and (b) Euler angle roll, (c) and (d) pitch, and (e) and (f) yaw.

now adopted in this retrieval algorithm. As shown in Fig. 3, from the samples B and C identified around the coastline along in-track/cross-track direction, the Euler angle roll/pitch for correcting the cross-track/in-track error at this FOV can be retrieved. The objective function for retrieving roll and pitch is established as follows:

$$\min \sum_{i=1}^{N} \left| \vec{b}'_{\mathrm{SC}} - \mathrm{ROT}_j\left(\xi_j^k\right) \cdot \vec{b}_{\mathrm{SC}} \right|_{l_2}^2 \quad -\frac{\pi}{2} \le \xi_j^k \le \frac{\pi}{2}, \;\; j = r, p; \;\; k = 1 \sim 96 \quad (11)$$

where ξ_j^k is the Euler angle roll or pitch for the kth FOV, N is the number of samples around the kth FOV, $\vec{b}_{\mathrm{SC}}$ and $\vec{b}'_{\mathrm{SC}}$ are the view vectors derived from the samples identified by the above strategy, and $\mathrm{ROT_j}$ is the rotation matrix corresponding to the jth Euler angle defined in (4). The limited-memory Broyden–Fletcher–Goldfarb–Shanno (L-BFGS-B) algorithm is applied to solve this nonlinear optimization problem with simple bounds. This algorithm, which is based on the gradient method, uses a limited-memory BFGS matrix to approximate the Hessian matrix of the objective function [23]. In this

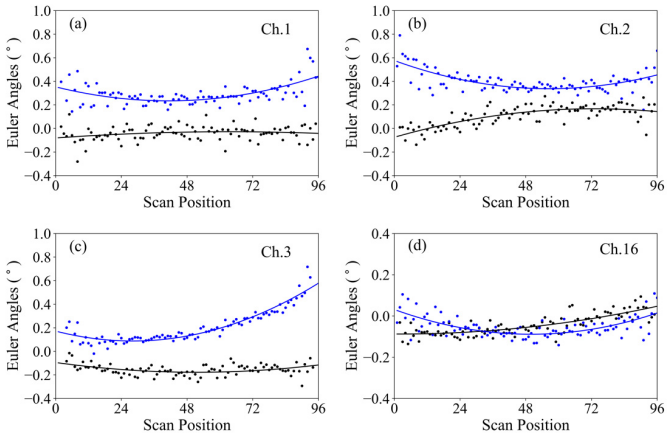

Fig. 9. Retrieved Euler angle roll (black points) and pitch (blue points) at each scan position of SNPP ATMS channel 1(a), 2(b), 3(c), and 16(d). Black and blue lines are the secondary polynomial fitting lines of the points with the same color.

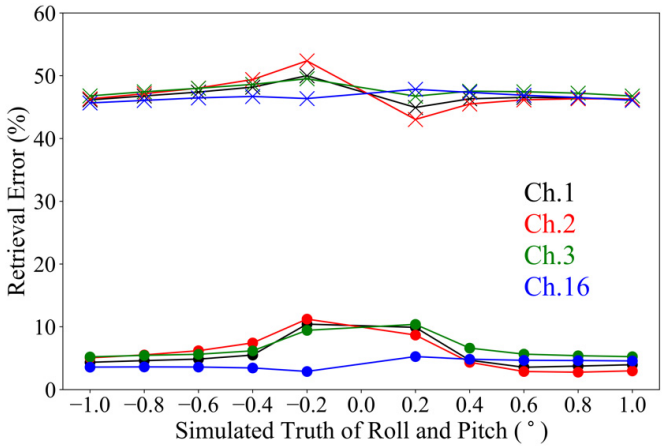

Fig. 10. Variation of retrieval error with the simulated truth of Euler angles. The retrieval error is defined as the average of the relative error of the two Euler angles. Circle and cross with solid lines are the retrieval error of the algorithm with and without the separate-domain technique, respectively.

paper, the iteration of L-BFGS-B always begins from an initial guess of zero. By selecting specific inflection points in specific domains, the boresight pointing Euler angles can be retrieved independently, and thus, the bias in the data can be reduced. Note that since the geolocation error detected by CIP method is the total residual static error, the retrieved Euler angles actually represent the boresight pointing misalignment caused by all the possible static error sources.

B. On-Orbit Boresight Pointing Error Retrieval Results and Accuracy Evaluation

The data set 2016 which has been used in Section III-B to estimate the on-orbit geolocation error of SNPP ATMS is now used in the retrieval algorithm in (11) to derive the boresight pointing Euler angles. The retrieved Euler angles of the four window channels are presented in Fig. 9. To reduce the uncertainty, the retrieved roll/pitch of each channel is fit by a quadratic polynomial function and the Euler angle at each FOV on the fitting line is taken as the final solution, as shown in Fig. 9. The retrieved Euler angles appear obvious scan-angle-dependent and band-dependent feature, which indicates that the antenna beam misalignment is one of the major error sources of the static geolocation error and the correction matrix determined by prelaunch ground test is incapable of effectively eliminating the geolocation error caused by such error source.

To evaluate the accuracy of the retrieval algorithm and verify the effectiveness of the separate-domain technique, sensitivity experiment is designed as follows. First, a series of observations with known geolocation errors are generated. For each observation, $\vec{b}_{\mathrm{SC}}$ is derived from the raw geolocation data following (5)–(10), corrected by the matrix $\mathrm{ROT}_{\mathrm{corr}}$ created from the retrieved Euler angles presented in Fig. 9, and then rotated by the matrix $\mathrm{ROT}^{\mathrm{T}}_{\mathrm{simu}}$ created from the predetermined Euler angles

$$\vec{b}'_{\mathrm{SC}} = \mathrm{ROT}^{\mathrm{T}}_{\mathrm{simu}} \cdot \mathrm{ROT}_{\mathrm{corr}} \cdot \vec{b}_{\mathrm{SC}}. \tag{12}$$

$\vec{b}'_{\mathrm{SC}}$ is then transferred back to the ground geolocation latitude and longitude following the normal geolocation process. Second, the retrieval algorithm with and without separate-domain techniques is applied to the contaminated geolocation data set, respectively. Without separate-domain technique, the two Euler angles are indiscriminately and simultaneously retrieved from the samples derived from all regions. The retrieval accuracy is estimated by comparing the retrieved Euler angles and the known truth. The retrieval error is defined as the average of the relative error of the two Euler angles. The data set 2016 is used in this sensitivity study. The Euler angles of simulated truth are set from $-1°$ to $1°$ at $0.2°$ intervals, except at $0°$. The sensitivity study result is presented in Fig. 10. It can be seen that by using the separate-domain technique, the retrieval error can be reduced from 47% to 5% on average.

V. On-Orbit Correction of SNPP ATMS Geolocation Error

From the retrieved boresight pointing Euler angles in Fig. 9, the pointing error correction matrices $\mathrm{ROT}_{\mathrm{Corr}}$ for on-orbit SNPP ATMS geolocation can be built through (4). The correction matrices can then be applied to improve the on-orbit geolocation accuracy by updating the instrument mounting matrix which is stored in the geolocation input parameter file

$$\mathrm{ROT}^{\mathrm{new}}_{\mathrm{SC/INST}} = \mathrm{ROT}_{\mathrm{Corr}} \cdot \mathrm{ROT}^{\mathrm{org}}_{\mathrm{SC/INST}} \tag{13}$$

where $\mathrm{ROT}^{\mathrm{org}}_{\mathrm{SC/INST}}$ and $\mathrm{ROT}^{\mathrm{new}}_{\mathrm{SC/INST}}$ are the original and updated instrument mounting matrices. Since the retrieved Euler angles represent the boresight pointing misalignment caused by all the possible static error sources, the correction matrices actually correct the total static part of the geolocation error.

To independently verify the effectiveness of these correction matrices, a different data set of SNPP ATMS in June, July, and August of 2014 (Data 2014) is used to estimate the in-track and cross-track geolocation errors before and after correction. The result is shown in Fig. 11. The in-track and cross-track errors near nadir and edges of the scan are averaged and listed in Table II.

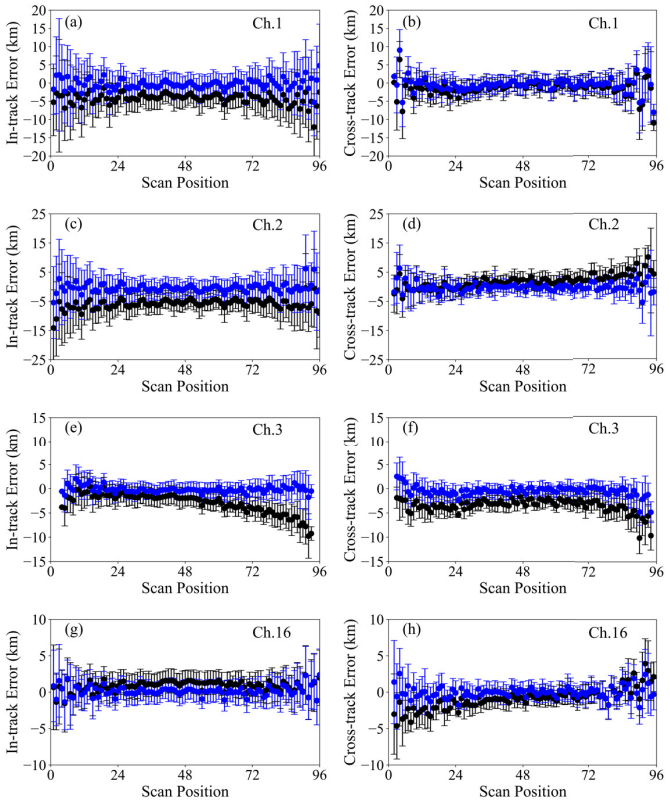

Fig. 11. FOV-dependent geolocation error of SNPP ATMS channel 1(a–b), 2(c–d), 3(e–f), and 16(g–h) before and after applying the correction matrices. Black points with error bar are the mean value and standard deviation of the geolocation error derived from the statistics on the raw observations in data set 2014. Blue points with error bar are the same as the black ones except that the observations are corrected by the correction matrices constructed by the Euler angles retrieved from data set 2016.

It can be seen that by applying the correction matrices, the scan-angle-dependent feature in geolocation error is largely removed. After correction, the in-track and cross-track geolocation errors are reduced on the FOVs both near nadir and toward the end of scan lines, except the cross-track error at FOV 1–5 of channel 2. The total geolocation error at nadir before/after correction is 3.8/0.8 km at K-band, 5.6/0.8 km at Ka-band, 3.3/0.4 km at V-band, and 1.5/0.1 km at W-band. The geolocation bias at the edge of the scan line before/after correction is 4.6/1.3 km at K-band, 9.4/1.8 km at Ka-band, 4.4/2.4 km at V-band, and 3.2/0.8 km at W-band. After correction, the total geolocation bias at nadir is much less than the prelaunch established specification for SNPP ATMS. Overall, the correction near nadir is better than that at large scan angles. This is because of the fact that the FOV size at large scan angle is much larger than that near nadir, which not only decreases the number of samples but also increases the uncertainty in those samples with large scan angles.

TABLE I

REGIONAL DISTRIBUTION OF QUALIFIED RETRIEVAL SAMPLES OF DATA SET 2016

Region Index	Ch.1	Ch.2	Ch.3	Ch.16
1	953	1010	858	1015
2	333	359	348	332
3	154	176	165	180
4	77	86	70	81
5	13	32	43	15
6	13	54	56	22
7	212	223	200	220
8	102	111	110	115
9	140	150	146	138
10	191	220	205	184
11	1051	1069	970	1077
12	103	112	106	82
13	376	390	321	356
14	355	382	302	321
15	1073	1159	1003	1085
16	1696	1798	1518	1667
17	176	193	164	146
18	37	52	38	29
19	74	80	71	68
20	285	314	266	257
21	447	487	455	478
22	39	49	53	42
23	132	207	169	98
24	445	463	434	456
Total	8477	9176	8071	8464

TABLE II

GEOLOCATION ERROR ESTIMATED FROM DATA SET 2014 BEFORE AND AFTER THE CORRECTION OF THE EULER ANGLES RETRIEVED FROM DATA SET 2016

Ch.	Ground Geolocation Error (km) Before / After correction					
	In-Track		Cross-Track		Total	
	FOV 1-5	FOV 46-50	FOV 1-5	FOV 46-50	FOV 1-5	FOV 46-50
1	-4.4 / 0.4	-3.7 / -0.6	-1.6 / 1.2	-0.6 / -0.5	4.6 / 1.3	3.8 / 0.8
2	-9.4 / -1.3	-5.3 / -0.7	-0.8 / 1.2	1.8 / -0.4	9.4 / 1.8	5.6 / 0.8
3	-3.9 / -1.0	-2.2 / -0.2	-2.7 / 2.2	-2.6 / -0.3	4.4 / 2.4	3.3 / 0.4
16	-0.2 / 0.1	1.3 / 0.1	-3.2 / 0.8	-0.9 / -0.008	3.2 / 0.8	1.5 / 0.1

VI. CONCLUSION AND DISCUSSION

The analysis of this paper shows that for SNPP ATMS, the static error term with scan-angle-dependent feature is a dominant part among all the geolocation error sources. This boresight pointing error can be corrected by the Euler angle roll and pitch defined in SC system at each scan position. A mathematical model is developed to describe the boresight pointing error with such special pattern and connect it with the ground geolocation error. To monitor and reduce the on-

orbit geolocation error, a retrieval algorithm for boresight pointing Euler angles is established based on the geolocation mathematical model and a refined CIP method. In this retrieval algorithm, Euler angler roll and pitch are retrieved for each FOV position of each window channel. The separate-domain technique is developed to mitigate the uncertainties in CIP method. Numerical simulation results show that by using this technique, the retrieval error can be reduced from 47% to 5%. Boresight pointing Euler angles are retrieved by this new algorithm from ATMS TDR in June, July, and August of 2016. The retrieval result is independently validated through a different TDR data set in June, July, and August of 2014. By using the correction matrix built by the retrieved Euler angles, the geolocation error is obviously reduced both at nadir and at the edge of the scan. The total geolocation error at nadir before/after correction is 3.8/0.8 km at K-band, 5.6/0.8 km at Ka-band, 3.3/0.4 km at V-band, and 1.5/0.1 km at W-band. The geolocation bias at the edge of the scan line before/after correction is 4.6/1.3 km at K-band, 9.4/1.8 km at Ka-band, 4.4/2.4 km at V-band, and 3.2/0.8 km at W-band. The total geolocation error at nadir is much less than ATMS designed specifications. The scan-angle-dependent feature observed in the geolocation error is also largely reduced.

Several factors may contribute to the uncertainty of the retrieval algorithm developed in this paper. As described in the separate-domain technique, the selected coastlines should be strictly aligned with the in-track or cross-track directions. In reality, it is impossible to find a coastline that perfectly meets such requirement. This will lead to the residual bias in the identified ground "truth." Besides, the sharp decrease in the FOV resolution toward the ends of the scan of ATMS will increase the uncertainties in the retrieval samples. Apart from these factors, the observation noise and point spread function of ATMS also induce uncertainties in the location of the observed coastline points. More efforts need to be made to quantitatively distinguish the uncertainties related to these specific factors. The CIP method is inapplicable to the atmosphere opaque channels. For these channels, a new method is required to identify the reliable geolocation reference targets. This paper shows that SNPP ATMS geolocation error is mainly contributed by both the antenna beam misalignment and the instrument mounting error. However, to further identify the amount of bias, each internal interface of the instrument could cause is beyond the capability of CIP method. Furthermore, the retrieved Euler angles appear obvious scan-angle-dependent feature which indicates that the measurements of antenna beam alignment with respect to the instrument cube during the prelaunch ground test should be made at more scan positions besides FOV 1, 48, and 96. In our future work, we will study on these topics together with the instrument vendor to further improve ATMS geolocation accuracy.

It should be noted that the geolocation error mathematical model and the Euler angle retrieval algorithm developed in this paper are not limited to ATMS. For any transparent window channel of space borne microwave observations, they can be used to retrieve the boresight pointing error and build the correction matrices to improve the on-orbit geolocation accuracy. This algorithm will be implemented to NOAA Integrated Calibration/Validation System Long-Term Monitoring to monitor the long-term variation of ATMS geolocation accuracy.

REFERENCES

[1] F. Weng, X. Zou, X. Wang, S. Yang, and M. D. Goldberg, "Introduction to Suomi National Polar-Orbiting Partnership advanced technology microwave sounder for numerical weather prediction and tropical cyclone applications," *J. Geophys. Res*, vol. 117, no. D19, p. 112, Oct. 2012.

[2] Y. Han, F. Weng, X. Zou, H. Yang, and D. Scott, "Characterization of geolocation accuracy of Suomi NPP advanced technology microwave sounder measurements," *J. Geophys. Res.*, vol. 121, no. 9, pp. 4933–4950, 2016, doi: 10.1002/2015JD024278.Apr. 2016.

[3] F. Tang, X. Zou, H. Yang, and F. Weng, "Estimation and correction of geolocation errors in FengYun-3C microwave radiation imager data," *IEEE Trans. Geosci. Remote Sens.*, vol. 54, no. 1, pp. 407–420, Jan. 2016.

[4] *Advanced Technology Microwave Sounder (ATMS) Calibration Data Book*, document ATMS PFM P/N 1362460-1 S/N 302, Northrop Grumman, Azusa, CA, USA, Mar. 2007.

[5] L. H. Hoffman, W. L. Weaver, and J. F. Kibler, "Calculation and accuracy of ERBE scanner measurement locations," NASA Langley Res. Center, Hampton, VI, USA, Tech. Rep. NASA-TP-2670, 1987, pp. 1–34.

[6] G. L. Smith, K. J. Priestley, P. C. Hess, C. Currey, and P. Spence, "Validation of geolocation of measurements of the clouds and the earth's radiant energy system (CERES) scanning radiometers aboard three spacecraft," *J. Atmos. Ocean. Technol.*, vol. 26, pp. 2379–2391, Mar. 2009.

[7] D. T. Gregorich and H. H. Aumann, "Verification of AIRS boresight accuracy using coastline detection," *IEEE Trans. Geosci. Remote Sens.*, vol. 41, no. 2, pp. 298–302, Feb. 2003.

[8] J. C. Currey, "Geolocation assessment algorithm for CALIPSO using coastline detection," Nat. Aeronaut. Space Admin. (NASA) Langley Res. Center, Hampton, VI, USA, Tech. Rep. NASA/TP-2002-211956, 2002, pp. 1–27.

[9] L. Wang *et al.*, "Geolocation assessment for CrIS sensor data records," *J. Geophys. Res. Atmos.*, vol. 118, no. 22, pp. 12, 690–12, 704, Nov. 2013.

[10] L. Wang, B. Zhang, D. Tremblay, and Y. Han, "Improved scheme for Cross-track Infrared Sounder geolocation assessment and optimization," *J. Geophys. Res., Atmos.*, vol. 122, no. 1, pp. 519–536, 2017, doi: 10.1002/2016JD025812.

[11] R. E. Wolfe *et al.*, "Achieving sub-pixel geolocation accuracy in support of MODIS land science," *Remote Sens. Environ.*, vol. 83, pp. 31–49, Nov. 2002.

[12] R. E. Wolfe, G. Lin, M. Nishihama, K. P. Tewari, J. C. Tilton, and A. R. Isaacman, "Suomi NPP VIIRS prelaunch and on-orbit geometric calibration and characterization," *J. Geophys. Res., Atmos.*, vol. 118, no. 20, pp. 11508–11521, 2013.

[13] K. V. Khlopenkov, A. P. Trishchenko, and Y. Luo, "Achieving subpixel georeferencing accuracy in the Canadian AVHRR processing system," *IEEE Trans. Geosci. Remote Sens.*, vol. 48, no. 4, pp. 2150–2161, Apr. 2010.

[14] R. Bennartz, "On the use of SSM/I measurements in coastal regions," *J. Atmos. Ocean. Technol.*, vol. 16, pp. 417–431, Apr. 1999.

[15] I. Moradi, H. Meng, R. R. Ferraro, and S. Bilanow, "Correcting geolocation errors for microwave instruments aboard NOAA satellites," *IEEE Trans. Geosci. Remote Sens.*, vol. 51, no. 6, pp. 3625–3637, Jun. 2013.

[16] G. A. Poe and R. W. Conway, "A study of the geolocation errors of the special sensor microwave/imager (SSM/I)," *IEEE Trans. Geosci. Remote Sens.*, vol. 28, no. 5, pp. 791–799, Sep. 1990.

[17] G. A. Poe, E. A. Uliana, B. A. Gardiner, T. E. Vonrentzell, and D. B. Kunkee, "Geolocation error analysis of the special sensor microwave imager/sounder," *IEEE Trans. Geosci. Remote Sens.*, vol. 46, no. 4, pp. 913–922, Apr. 2008.

[18] *Joint Polar Satellite System (JPPS) VIIRS Geolocation Algorithm Theoretical Basis Document (ATBD)*, document, Goddard Space Flight Center, Greenbelt, MD, USA, Jul. 2011.

[19] D. A. Vallado and W. D. McClain, *Fundamentals of Astrodynamics and Applications*, 4th ed. Hawthorne, CA, USA: Microcosm Press, 2013, pp. 461–467.
[20] G. Kaplan, J. Bartlett, A. Monet, J. Bangert, and W. Puatua, *User's Guide to NOVAS Version F3.1, Naval Observatory Vector Astrometry Software*, Fortran Edition, U.S. Naval Observatory, Washington, DC, USA, Mar. 2011.
[21] P. Wessel and W. H. F. Smith, "A global, self-consistent, hierarchical, high-resolution shoreline database," *J. Geophys. Res.*, vol. 101, no. B4, pp. 8741–8743, Apr. 1996.
[22] *Document for Common Geolocation Software*, Joint Polar Satellite System (JPSS) Operational Algorithm Description (OAD), May 2017.
[23] C. Zhu, R. H. Byrd, P. Lu, and J. Nocedal, "L-BFGS-B: Fortran subroutines for large-scale bound-constrained optimization," *ACM Trans. Math. Softw.*, vol. 23, no. 4, pp. 550–560, 1997.

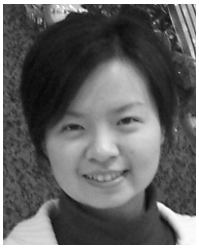

Jun Zhou (M'18) received the Ph.D. degree from the Institute of Atmospheric Physics (IAP), Chinese Academy of Sciences (CAS), Beijing, China, in 2010.

From 2010 to 2014, she was a Research Assistant with IAP, CAS, focusing on retrieving 3-D cloud structure through cloud tomography technique. From 2014 to 2015, she was a Visiting Scholar with the Earth System Research Laboratory, NOAA, Boulder, CO, USA, focusing on applying satellite data into data assimilation system. In 2015, she joined the Earth System Science Interdisciplinary Center, University of Maryland, College Park, MD, USA, where she is involved in the NPP/JPSS Advanced Technology Microwave Sounder geolocation and validation. Her research interests include the retrieval of atmospheric parameters from passive microwave data, satellite data assimilation, and satellite geolocation and validation.

Hu Yang (M'09) received the Ph.D. degree from the Institute of Remote Sensing Application, Chinese Academy of Sciences, Beijing, China, in 2003.

From 2003 to 2011, he was a Senior Research Scientist with the National Satellite Meteorological Center, China Meteorological Administration, Beijing, leading the microwave instrument calibration and satellite ground application system development as the Instrument Scientist and the Program Scientist. In 2012, he joined the Earth System Science Interdisciplinary Center, University of Maryland, College Park, MD, USA, focusing on NPP/JPSS ATMS calibration/validation as a Project PI. He has authored over 40 peer-reviewed journals. His research interests include passive microwave radiometer calibration/validation, satellite geolocation, and satellite observation simulation.

Kent Anderson received the B.S. and M.S. degrees in electrical engineering from the Rose-Hulman Institute of Technology, Terre Haute, IN, USA, in 1971 and 1972, respectively.

He has 30-year experience in systems engineering for spaceborne remote sensing systems. For the last 15 years, he has been the Lead Systems Engineer for Civil Space Programs with Northrop Grumman Electronic Systems, Azusa, CA, USA, focused primarily on millimeter-wave radiometry, particularly for the ATMS program. His research interests include requirements management, initial design trade studies, performance analyses, and analyses of test data.